Research Field: **Outdoor environment**
Research Year: FY2020
Research Number: 20202012
Research Theme:
The catch ratio and runoff behavior of wind-driven rain on different building envelope materials

Representative Researcher: **Huibo Zhang**

Budget [FY2020]: **400,000** Yen

*There is no limitation of the number of pages of this report.
*Figures can be included to the report and they can also be colored.
*Submitted reports will be uploaded to the JURC Homepage.

1. Research Aim

- To clear the distribution law of wind-driven rain (WDR) intensity reaching building facades caused by different rainfall events.
- To explore the interaction mechanism between the external surface materials and raindrops under different wind-drive rain parameters, then to master the variation characteristics of rainwater runoff and moisture accumulation caused by WDR after hitting the exterior wall.
- To provide accurate moisture boundary conditions for building performance simulation.

2. Research Method

(1) Field Measurement;

1) Measurement setup

Generally, building structures are complex, and large-scale measurements are accordingly time- and labor-intensive. Moreover, the relationship of WDR distribution with building type and rain features is also complicated. With these limitations in mind, an experimental house (length, 146.5 cm; width, 117 cm; height, 210 cm) was built and placed at Shanghai Jiao Tong University, to permit universal and representative WDR measurement (Fig.1(a)). The southern and eastern sides of the experimental house were relatively open, and a few small trees and grass are present on the north side. Considering measurements were recorded in the rainy summer and autumn seasons when the eastern-to-southern winds prevail, the façade facing the east was selected for measurement. Fig. 1 shows the experimental house layout and diagram of the surrounding environment.

(a) 

(b) 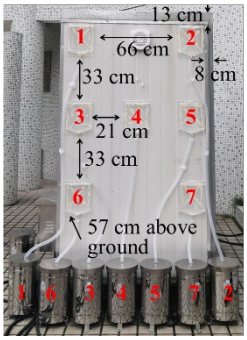

Figure 1. (a) Experiment house; (b) Layout of WDR gauges

Wind speed and direction were measured using a 3D ultrasonic anemometer (R.M. Young Company; MI, USA), with measurement capabilities from 0.00–40.00 m/s, and 0.0–360.0°, respectively.

The horizontal rainfall amount and WDR amount were measured using RS-YL-N01-4 tipping bucket rain gauges (Kenda People's Corporation; Jinan, China), with 0.2 mm accuracy. The theoretical volume of a single tipping bucket was 6.28 mL, and the measured rainfall intensity ranged from 0–4 mm/min. Two rain gauges were used to verify the reference value of the horizontal rainfall amount during the measurement period: (A) was located close to the tripod, and (B) was located to the south side of the experimental house (Fig.1).

Fig. 2 shows the self-designed, polymethyl methacrylate (PMMA) WDR gauge, with a collection area of 0.18× 0.18 cm^2, and silica gel hose connection to the rain gauge. Fig. 1(b) shows the distribution of the WDR gauges on the measured wall façade. As the wind flows into the building, the flow patterns of the wall edges are more complex than those in the wall center; therefore, three WDR gauges were arranged on each the left and right sides of the measured wall façade, while one was placed in the middle. During measurement, outdoor temperature and relative humidity were also recorded, and all data were recorded at 1 min intervals.

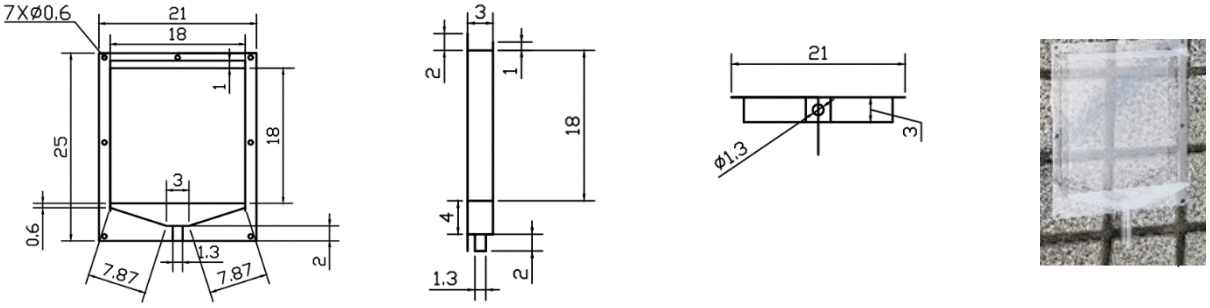

(a) (b) (c) (d)

Figure 2. WDR gauge specifications (in cm): (a) Front view; (b) Side view; (c) Top view; and, (d) Actual view.

2) Measurement errors

There were likely multiple sources of error with the WDR measurements, such as residual rainwater evaporation in the collection area, rainwater retention on the surface of the rain gauge tipping bucket, rain splash, rain condensation, and wind turbulence on the WDR gauge. Bloken [1] found that, except for extreme storms, the influence of wind on the measured errors of WDR can generally be ignored. Further, the author stated that for a WDR gauge made of PMMA, and an area of 0.2×0.2 m^2, the adhesive rainwater on the surface of the collection area was maintained at 0.10 L/m^2.

In the measurements here, the height of the edge of the WDR collection area largely avoided the influence of wind. In addition, the measurement periods in the Shanghai summer and autumn maintain high humidity levels, with limited evaporative capacity, when it rains. Therefore, the influence of wind on the collection of WDR, condensation in the collection area, and the evaporation of rainwater during rainfall can all be ignored; however, the adhesion error caused by the connecting silica gel hose surface must be considered. On the whole, there are three primary error sources in this measurement: (1) evaporation of the adhesion water on the WDR gauge collection surface, E_{aw}; (2) adhesion water error of the pipe, E_{tu}; and (3) adhesion water error of the tipping bucket, E_{rw}. Thus, the total measurement error (E_{tot}) of each WDR measurement was calculated according to Eq. (1):

$$E_{tot} = E_{aw} + E_{tu} + E_{rw} \quad (1)$$

The relative error (E_{re}) was calculated according to Eq. (2):

$$E_{re} = \frac{E_{tot}}{S_{wdr-i}} \quad (2)$$

where $S_{wdr\text{-}i}$ (i = 1–7) is the WDR amount collected at an individual measuring point.

The three error values were systematically assessed before the start of the measurement periods. The average value of E_{aw} was 0.108 L/m^2, and Table 1 shows E_{tu} and E_{rw} for each measuring point.

Table 1. Measurement errors (in mm) associated with: E_{tu}, adhesion water error of the pipe; and E_{rw}, adhesion water error of the tipping bucket.

Measurement points	1	2	3	4	5	6	7	A	B
E_{tu}	0.030	0.049	0.020	0.053	0.015	0.050	0.032	-	-
E_{rw}	0.046	0.009	0.000	0.009	0.056	0.000	0.006	0.000	0.034

The WDR catch ratio was a cumulative result after considering the measured error, and is expressed as a percentage according to Eq. (3):

$$\eta' = \eta + \eta_{error} = \frac{S_{wdr} + E_{tot}}{S_h} \quad (3)$$

where η' is the catch ratio of the measuring point obtained by dividing the sum of the WDR amount (S_{wdr}) and the total error (E_{tot}), by the horizontal rainfall amount (S_h).

3) Data processing method

The present study recorded meteorological data at 10 min intervals (unless stated otherwise) in accordance with previous research [2]. Data of wind elevation, speed, and direction during rain events were 10 min averages. The rainfall and WDR amounts were totaled values taken within 10 min of each other. The effective wind direction, φ_{eff}, wind speed, U_{eff}, and rainfall intensity, $R_{h,eff}$, were calculated for each rain event. The effective wind direction was weighted by the tangential, $U_{t,eff}$, and the normalized effective wind velocities, $U_{n,eff}$, thus preventing errors caused by wind fluctuations in opposite directions. These parameters were calculated using Eqs (4–7):

$$\varphi_{eff} = \tan^{-1}\left(\frac{U_{t,eff}}{U_{n,eff}}\right) \tag{4}$$

$$U_{t,eff} = \frac{\sum R_h U_t}{\sum R_h}, \quad U_{n,eff} = \frac{\sum R_h U_n}{\sum R_h} \tag{5}$$

$$U_{eff} = \sqrt{\left(U_{t,eff}\right)^2 + \left(U_{n,eff}\right)^2} \tag{6}$$

$$R_{h,eff} = \frac{\sum R_h}{n} \tag{7}$$

where U_t is the tangential velocity, U_n is the normalized velocity, R_h is the rainfall intensity, and n is the number of times the horizontal rainfall intensity (R_h) > 0.

(2) Semi-empirical evaluation method;

The ISO 15927-3:2009 [3] and ASHRAE 160-2016 standards [4] are two semi-empirical models often used to assess WDR façade exposure.

1) ISO model

In the ISO model, WDR intensity is defined according to Eq. (8):

$$R_{wdr} = \frac{2}{9} U_{10} C_R C_T O W R_h^{\frac{8}{9}} \cos\theta \tag{8}$$

where 2/9 is the WDR coefficient (s/m); U_{10} is the reference wind speed at a height of 10 m (m/s); C_R is the roughness coefficient; C_T is the terrain coefficient; O is the obstruction factor, reflecting the effect of the surrounding environment on the calculated wall façade; W is the wall factor, which can be used to evaluate the degree of influence of the wall façade by the WDR; R_h is the hourly rainfall amount (mm/h); and, θ is the angle between the wind direction and the direction normal to the wall.

2) ASHRAE model

The ASHRAE model uses the rain exposure and rain deposition factors to calculate the amount of WDR striking on the building façade. The WDR intensity in the model is defined according to Eq. (9):

$$R_{wdr} = F_D F_E F_L U_{10} R_h \cos\theta \tag{9}$$

where F_D is the rain deposition factor, F_E is the rain exposure factor, F_L is an empirical constant (0.2 kg·s/(m^3·mm)), and other parameters are the same as Eq. (8).

(3) Numerical Simulation.

The numerical simulation of wind-driven rain involves the theory of multiphase flow. There are two commonly used methods of wind-driven rain numerical simulation: Lagrangian particle tracking method (DPM method) and Eulerian multiphase method (EM method). Because the volume of raindrops in the air is much smaller than that of air, the numerical simulation selects the more appropriate DPM method.

The DPM method regards wind as a continuous phase and raindrops as a discrete phase. After the continuous phase calculation converges, the catch ratio is calculated by tracking the trajectory of raindrop particles.

As the continuous phase in the WDR field, Realizable k-ε model was selected as the governing

equation of the wind phase. For the rain phase, it is assumed that the raindrop is an ideal sphere particle, and the evaporation, deformation and fragmentation of the raindrop in the process of falling are ignored, then the motion trajectory equation of a single raindrop is as follows:

$$m\frac{d^2x}{dt^2}=3\pi\mu D\left(U-\frac{dx}{dt}\right)\frac{C_D\,\mathrm{Re}}{24} \quad (10)$$

$$m\frac{d^2y}{dt^2}=3\pi\mu D\left(V-\frac{dy}{dt}\right)\frac{C_D\,\mathrm{Re}}{24} \quad (11)$$

$$m\frac{d^2z}{dt^2}=3\pi\mu D\left(W-\frac{dz}{dt}\right)\frac{C_D\,\mathrm{Re}}{24}+mg\left(\frac{\rho_a-\rho_w}{\rho_w}\right) \quad (12)$$

Where, U, V and W are the components of wind speed in X, Y and Z directions respectively; m is the mass of a single raindrop, kg; μ is the dynamic viscosity of air; D is raindrop diameter; Re is the relative Reynolds number of wind and rain; C_D is the drag coefficient of raindrops; g is the acceleration of gravity, take -9.81 m/s^2; ρ_a is air density, take 1.225 kg/m^3; ρ_w is the density of raindrops, take the density of liquid water, 1000 kg/m^3.

3. Research Result

(1) Field Measurement

Fig. 3 shows the distribution of rainfall amount and wind over the study period (10 min averages). Rain was relatively frequent at the beginning of the analysis, occurring nearly daily before July 20. During this period, Shanghai is at the end of the "plum rainy season," dominated by continuous, but light to moderate rain, with low wind speeds. By the end of August and early September, rainfall amounts were high, but the time intervals between events were longer, slowly tapering off towards the end of the month. During the measurement period, the wind speed was maintained between 0–1.5 m/s, the maximum horizontal wind speed exceeded 2.5 m/s (August 4), and minimum was near zero. Wind direction fluctuated around 180°, with a tighter range observed from late July to late August.

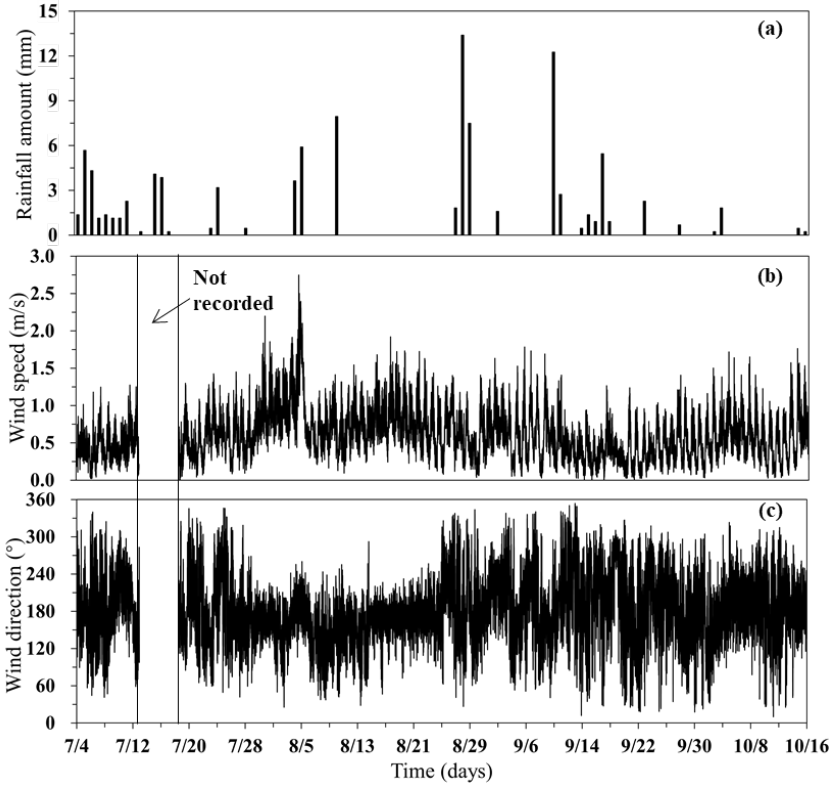

Figure 3. (a) Rainfall intensity, (b) wind speed, and (c) wind direction over the measurement period from July–October 2020.

Fig. 4 shows the frequency distribution of rainfall intensity (10 min averages), wind speed (1 min averages), and wind direction (1 min averages) over the analysis period. Rain hours refers to the total time when horizontal rainfall was being registered. The maximum rainfall intensity reached approximately 80 mm/h, intensities ≤ 16 mm/h accounted for > 95%, and intensities from 4–8 mm/h accounted for ~10%, indicating that light rain to moderate rain prevailed during the measurement period (Fig. 4(a)). Wind speed was ≤ 2.5 m/s in most cases, with an observed maximum of ~10 m/s (Fig. 4(b)). In rain hours, wind speeds ≤ 1.0 m/s account for ~90% of those recorded, and the cumulative frequency distribution curve of wind speed in rain hours lags behind all hours at the same wind speed distribution interval. Thus, lower wind speeds were predominant during rain hours across the measurement period. The prevailing wind directions were mainly from the southeast to southwest during both rain hours and non-rain hours (Fig. 4(c)). The direction frequency distribution of the SSE wind in rain hours was lower than that across all hours of the observation period, whereas SSW winds were predominant during rain hours.

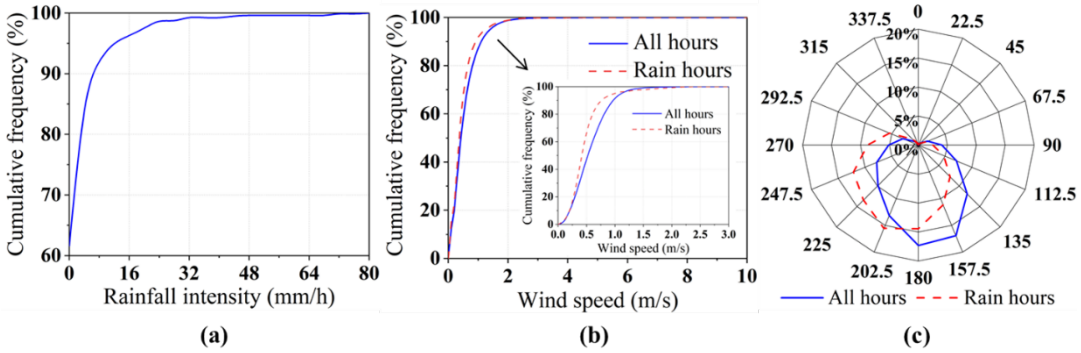

Figure 4. The cumulative frequency distributions of: (a) rainfall intensity, (b) wind speed, and (c) wind direction.

Fig. 5 presents the relationship among total rainfall amount, effective wind direction, effective rainfall intensity, and effective wind speed for each rain event ≥ 1 mm from during the analysis period (including rain events not collected WDR). Bubble size is proportional to the total rainfall amount, and bubble color correlates to the effective wind speed. Effective rainfall intensity was primarily observed between 2–8 mm/h, concentrating around 4 mm/h. Only one rain event was observed with an intensity > 10 mm/h. The effective wind speed range was 0–1.5 m/s, and effective wind direction was concentrated between the S–SSW throughout the analysis period.

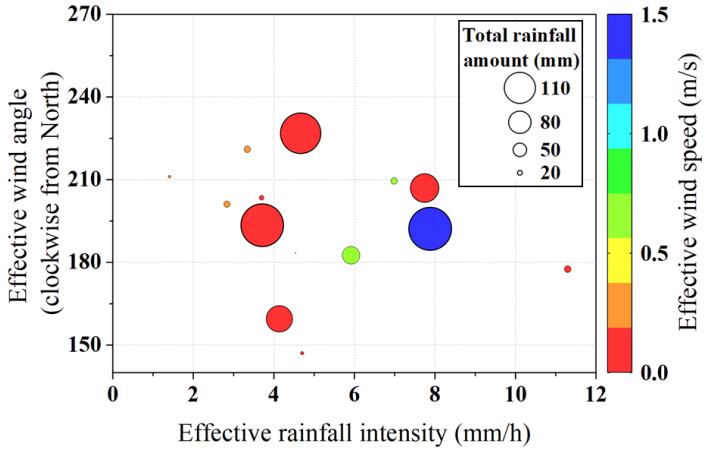

Figure 5. Relationship among total rainfall amount, effective wind direction, rainfall intensity, and wind speed for each rain event.

There were nine rain events with WDR records during the measurement period, spanning different characteristics; for example, short-term heavy rainfall, rain caused by "typhoon", and long-term light-to-moderate rainfall. Moreover, the error range of each measurement point ranged from 6–150%, which was in line with the WDR measurement characteristics described by Blocken and Straube [5]. The following is an analysis of five, WDR-recorded rain events, including meteorological data, the change in WDR amount over time, WDR catch ratio, and the corresponding measurement error. Table 2 shows the pertinent information for these rain events.

Table 2. Overview of the five rain events selected for deeper discussion. S_h is the total horizontal rainfall amount, and *TT* is the duration of the single rain event.

Number	U_{eff} (m/s)	φ_{eff}	$R_{h,eff}$ (mm/h)	Start time	End time	*TT*	S_h (mm)	Type
1	1.5	192°	7.88	8/4/2020 18:00	8/5/2020 11:00	17 h	118.0	Heavy rainfall with typhoon
2	0.7	186°	6.99	8/10/2020 17:00	8/10/2020 22:00	5 h	17.5	Short-term heavy rainfall
3	0.3	207°	7.74	8/28/2020 14:00	8/29/2020 14:00	24 h	79.0	Phased rainfall 1
4	0.8	183°	5.92	9/10/2020 18:00	9/11/2020 11:00	17 h	48.0	Phased rainfall 2
5	0.4	199°	4.33	9/16/2020 22:00	9/18/2020 15:00	41 h	88.0	Long time drizzle

Rain event 1: August 4–August 5, 2020

Fig. 6 (a–f) shows the changes in the meteorological parameters of across the 17 h of the Aug. 4–5 rain event. Initially, rainfall intensity and wind speed gradually increased, with three rainfall intensity peaks observed throughout the continuous rainfall. The maximum 10 min average wind speed reached 2.40 m/s, slowly decreasing after 21:00 on Aug. 4, and ultimately fluctuating near 1.0 m/s. Although the typhoon period brought strong winds and heavy rainfall, and the prevailing wind direction according to the rose diagram came from the SW, directionality changed steadily over time, fluctuating up to 200° across the entire rain event. The wind speed distribution frequency between 1.0–2.0 m/s was predominant and accounting for more than 70% of the proportion, followed by 2.0–3.0 m/s. The temperature and humidity "during rain" compared to immediately "before and after rain" showed a large difference. In the initial stage of rainfall, the temperature dropped rapidly and remained relatively low, near 25 °C. The average outdoor air temperatures during the same period pre-rain (Aug 2–3), during rain (Aug 4–5), and post-rain (Aug 6–7) were 31.2 °C, 25.7 °C, and 31.3 °C, respectively. Contrary to temperature, the “during rain” RH quickly climbed to 100.0% until the end of the rain event. The average values of RH in the same periods were 77.4%, 99.2%, and 85.5%, for pre-, during, and post-rain, respectively, with significantly higher levels post- rain than before.

Fig. 6(g) shows the measurement results of the WDR gauges and their catch ratios. As the rainfall progressed, the WDR amount at all measurement points increased. Generally, the WDR amount at the north side measured point was greater than that of the south side at the same height. RG5 on the north side collected the maximum WDR amount value, 2.7 mm, while the minimum value, 0.9 mm, appeared on the south side. Based on Fig. 6(d, f), the prevailing wind direction was SSW, with an effective angle of 192°. Therefore, when raindrops fall around the experimental house, their trajectory will be from south to north affected by the airflow, causing the WDR amount collected by the gauges on the south side to be generally lower at the same height. As shown in Fig. 6(g), the WDR catch ratio was relatively similar on north or south side, with the north side sites maintaining approximately three times greater ratios over the south. Among them, the catch ratio of RG4 was approximately twice that of RG3.

Table 3 shows the catch ratio and measurement error results for rain event 1. The evaporation times N related to E_{aw} was based on the assumptions in Section 2.2, and was comprehensively determined by the RH and rainfall changes during the measurement period. Because rainfall was continuous, and the average RH was > 99% throughout the rain event, the number of evaporations N = 1. The minimum and maximum relative errors were 6.0% and 21.9%, respectively; and the greater the amount of WDR collected, the smaller the relative error.

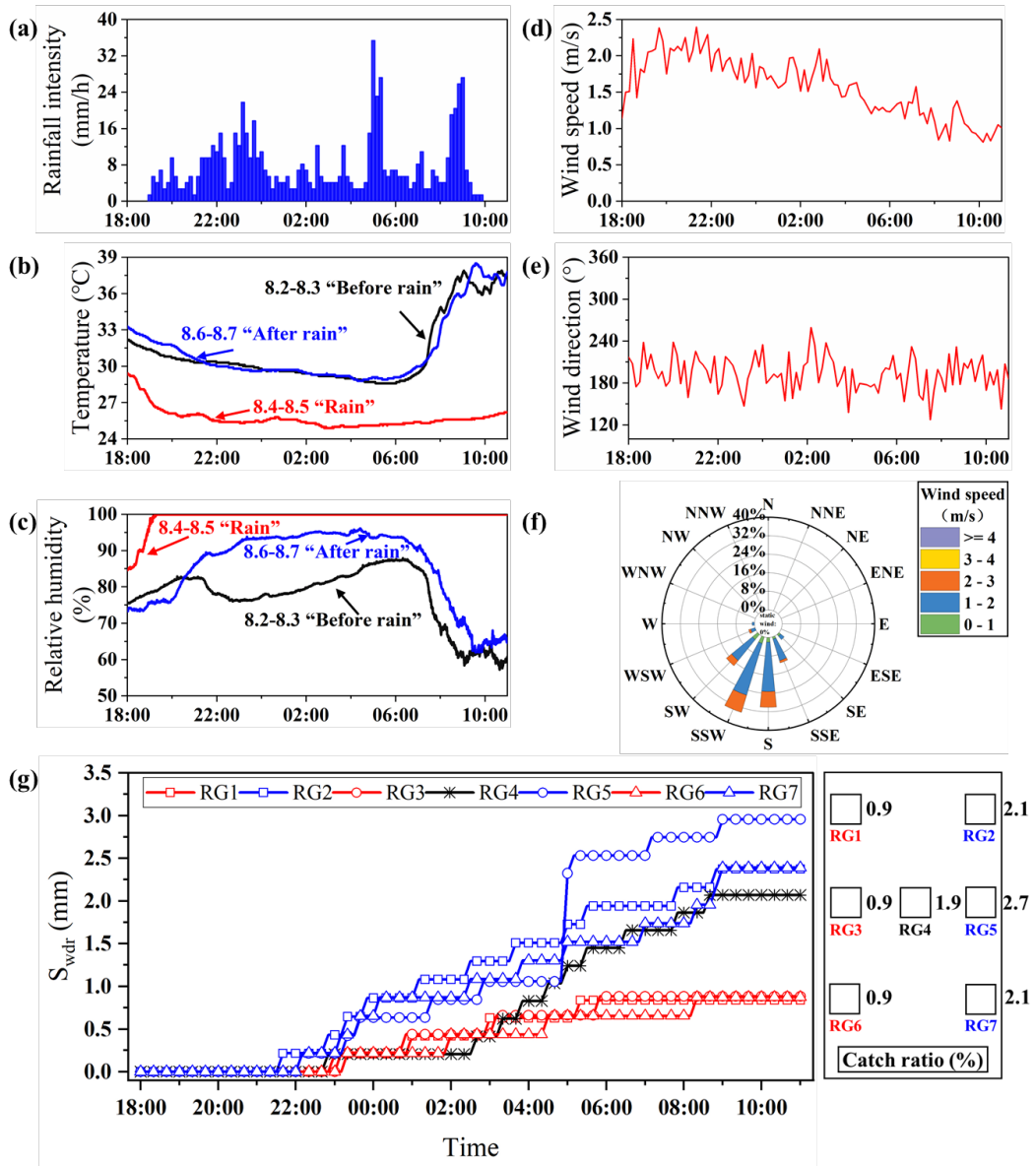

Figure 6. Patterns of Event 1, August 4–5, 2020: (a) Rainfall intensity; (b) Temperature; (c) Relative humidity; (d) Wind speed; (e) Wind direction; (f) Wind rose; (g) WDR amounts and catch ratios. The red lines represent all the measuring points on the south side of the measured wall façade, the blue lines represent all north side measuring points, and the black curve represents the middle No. 4 WDR measuring point.

Table 3. Results and errors of rain event 1.

Measurement point	Number of tips	S_{wdr} (mm)	E_{tot} (mm)	Relative error E_{tot}/S_{wdr}	η (%)	η' (%)
1	4	0.84	0.184	21.9%	0.7	0.9
2	11	2.37	0.166	7.0%	2.0	2.1
3	4	0.88	0.128	14.5%	0.7	0.9
4	10	2.07	0.170	8.2%	1.8	1.9
5	14	2.96	0.179	6.0%	2.5	2.7
6	4	0.87	0.158	18.2%	0.7	0.9
7	11	2.39	0.146	6.1%	2.0	2.1

(2) Semi-empirical evaluation method;

Fig. 7 shows a comparison between the two semi-empirical models and the measurement results. Because the ISO model does not provide a wall factor for a single-story, low-rise building, the average wall factor of a two-story building with a flat roof was considered here. The vertical axis catch ratio was the average value of each rain event's wall façade catch ratio, and showed that in rain event 1 and 5, both of which displayed relatively continuous rainfall intensities, the ISO model's results and the measured results were very close. For rain event 2 and 4, both marked by short-term, heavy rainfall in the early period when the majority of WDR was collected, the ASHRAE model's results were the most accurate.

Overall, the calculated results of the ISO model underpredicted the measured values by ~0.5–1.1 times, whereas the ASHRAE model's results overpredicted measurements by ~1.0–2.9 times. Through analysis, a significant difference was shown between the time resolution of the measurements and the semi-empirical models. The measured data were recorded at set intervals, and wind direction and speed continuously changed over time; while the semi-empirical models were the average values of weather data. In addition, the selection of the semi-empirical model parameters and the influence of the surrounding environment will cause modeled inaccuracies. For example, the ISO model does not account for the "wind-blocking effect" of adjacent buildings as an influential factor [6].

As a tool for quickly assessing the WDR distribution of building walls, semi-empirical models have been widely used in BE-HAM transmission models [7, 8]. The comparison results from the study here showed that semi-empirical model error is still an important factor, and care should be taken when using these models.

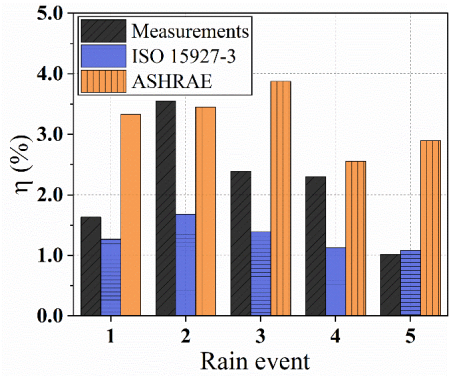

Figure 7. Comparison between semi-empirical models and measurements from the five rain events analyzed.

(3) Numerical Simulation.

From July 2020 to October 2020, the WDR measurement work was carried out. The validity verification of WDR selects the grab rate result of a certain rainfall time during the measured period. Figure 8 shows the comparison results between simulation and field measurement on a single facade of a building. The measured results are slightly lower than the simulated ones because the meteorological parameters vary from time to time during the measured period and there are certain errors in all the measured points. On the whole, the grabbing rates obtained by simulation and measurement are basically consistent in the spatial distribution trend, and the effectiveness of WDR is verified.

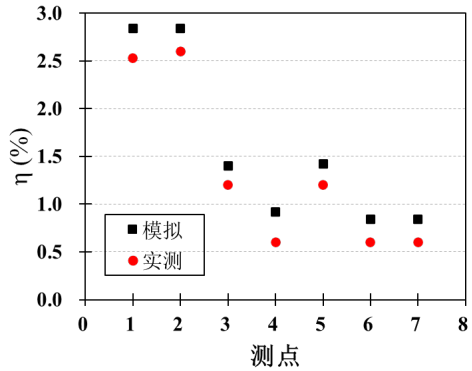

Figure 8 Comparison between WDR simulation and actual measurement

References

[1] B. Blocken, J. Carmeliet, On the accuracy of wind-driven rain measurements on buildings, Building and Environment 41(12) (2006) 1798-1810.
[2] B. Blocken, J. Carmeliet, On the errors associated with the use of hourly data in wind-driven rain calculations on building facades, Atmospheric Environment 41(11) (2007) 2335-2343.
[3] EN ISO 15927-3, Hygrothermal Performance of Buildings, Calculation and Presentation of climatic Data. Part 3: Calculation of a Driving Rain Index for Vertical Surfaces from Hourly Wind and Rain data, European Committee for Standardization, Brussels, 2009.
[4] ASHRAE 2016. ASHRAE standard 160-criteria for moisture control design analysis in buildings. AHSRAE, Atlanta, USA.
[5] J. Straube, Moisture control and enclosure wall systems, 1998.
[6] B. Blocken, G. Dezsö, J. van Beeck, J. Carmeliet, The mutual influence of two buildings on their wind-driven rain exposure and comments on the obstruction factor, Journal of Wind Engineering and Industrial Aerodynamics 97(5-6) (2009) 180-196.
[7] A. Fang, Y. Chen, L. Wu, Modeling and numerical investigation for hygrothermal behavior of porous building envelope subjected to the wind driven rain, Energy and Buildings 231 (2021) 110572.
[8] D. Chung, J. Wen, L.J. Lo, Development and verification of the open source platform, HAM-Tools, for hygrothermal performance simulation of buildings using a stochastic approach, Building Simulation 13(3) (2019) 497-514.

4. Published Paper etc.
[Underline the representative researcher and collaborate researchers]
[Published papers]
1. Tianda Qian, **Huibo Zhang***. Assessment of long-term and extreme exposure to wind-driven rain for buildings in various regions of China. ***Building and Environment***, 2021, 189: 107524.
2. Chao Chen, **Huibo Zhang***, Chi Feng, Yingli Xuan, Tianda Qian. Wind-driven rain on a low-rise building façade in Shanghai. ***Building and Environment***, submitted.

[Presentations at academic societies]
1. Huibo Zhang. Influence of different combination of wind and rain on the capturing rate of wind-driven rain on buildings. The 20th China HVAC Simulation Conference, April 8-9, 2021, Xi'an, China
2.

[Published books]
1.
2.

[Other]
Intellectual property rights, Homepage etc.

5. Research Group
1. Representative Researcher
Huibo Zhang
2. Collaborate Researchers
1. Yingli Xuan
2. Chao Chen
3. Tianda Qian

6. Abstract (half page)

Research Theme

The catch ratio and runoff behavior of wind-driven rain on different building envelope materials

Representative Researcher (Affiliation) **Huibo Zhang (Shanghai Jiao Tong University)**

Summary・Figures

Wind-driven rain (WDR) is a critical boundary condition for the thermal and moisture coupling calculations of buildings, and understanding its distribution patterning on façades is conducive to better designs of building envelope structures. Because there are few records of WDR measurements in China, this study conducted a high time resolution measurement of a low-rise experimental house in Shanghai, from July 4 to October 16, 2020. First, meteorological conditions were analyzed, including wind speed, wind direction, rainfall amount, rainfall intensity, temperature, and relative humidity, and five representative rain events were selected for further analysis. In addition to the meteorological data collected, the change in WDR amount over time, WDR catch ratio, and the corresponding measurement errors were assessed. Compared to non-rainy conditions, the temperature during rainfall was 4.0–5.6 °C lower, and relative humidity was 9.8–21.8% higher. The increase in rainfall amount and wind speed was conducive to an increase in WDR amount; and when the angle between the inflow wind direction and normal to the wall façade increased, the WDR catch ratio tended to decrease. The measurement relative errors had a negative exponential relationship with the WDR amount. Results were compared with two semi-empirical models, and showed that the ISO model was 0.5–1.1 times that of the measured values, while the ASHRAE model was between 1.0–2.9 times greater. Thus, when using semi-empirical models, attention may be paid to the influence and extent of model errors on the calculation results. The numerical simulation theory of DPM method is introduced, and then the validity of the wind and rain field in WDR simulation is verified.